Stem Cell Research & Therapy

RESEARCH

Open Access

The cytoskeleton dynamics-dependent LINC complex in periodontal ligament stem cells transmits mechanical stress to the nuclear envelope and promotes YAP nuclear translocation

Xuehuan Meng[1,2,3], Ye Zhu[1,2,3], Hao Tan[1,2,3], Baraa Daraqel[1,2,3,4], Ye Ming[1,2,3], Xiang Li[1,2,3], Guoyin Yang[1,2,3], Xinyi He[1,2,3], Jinlin Song[1,2,3*†] and Leilei Zheng[1,2,3*†]

Abstract

Background Periodontal ligament stem cells (PDLSCs) are important seed cells in tissue engineering and clinical applications. They are the priority receptor cells for sensing various mechanical stresses. Yes-associated protein (YAP) is a recognized mechanically sensitive transcription factor. However, the role of YAP in regulating the fate of PDLSCs under tension stress (TS) and its underlying mechanism is still unclear.

Methods The effects of TS on the morphology and fate of PDLSCs were investigated using fluorescence staining, transmission electron microscopy, flow cytometry and quantitative real-time polymerase chain reaction (qRT-PCR). Then qRT-PCR, western blotting, immunofluorescence staining and gene knockdown experiments were performed to investigate the expression and distribution of YAP and its correlation with PDLSCs proliferation. The effects of cytoskeleton dynamics on YAP nuclear translocation were subsequently explored by adding cytoskeleton inhibitors. The effect of cytoskeleton dynamics on the expression of the LINC complex was proved through qRT-PCR and western blotting. After destroying the LINC complex by adenovirus, the effects of the LINC complex on YAP nuclear translocation and PDLSCs proliferation were investigated. Mitochondria-related detections were then performed to explore the role of mitochondria in YAP nuclear translocation. Finally, the in vitro results were verified by constructing orthodontic tooth movement models in Sprague-Dawley rats.

Results TS enhanced the polymerization and stretching of F-actin, which upregulated the expression of the LINC complex. This further strengthened the pull on the nuclear envelope, enlarged the nuclear pore, and facilitated

†Leilei Zheng and Jinlin Song contributed equally to this work and are co-corresponding authors.

*Correspondence:
Jinlin Song
songjinlin@hospital.cqmu.edu.cn
Leilei Zheng
zhengleileicqmu@hospital.cqmu.edu.cn

Full list of author information is available at the end of the article

YAP's nuclear entry, thus enhancing the expression of proliferation-related genes. In this process, mitochondria were transported to the periphery of the nucleus along the reconstructed microtubules. They generated ATP to aid YAP's nuclear translocation and drove F-actin polymerization to a certain degree. When the LINC complex was destroyed, the nuclear translocation of YAP was inhibited, which limited PDLSCs proliferation, impeded periodontal tissue remodeling, and hindered tooth movement.

Conclusions Our study confirmed that appropriate TS could promote PDLSCs proliferation and periodontal tissue remodeling through the mechanically driven F-actin/LINC complex/YAP axis, which could provide theoretical guidance for seed cell expansion and for promoting healthy and effective tooth movement in clinical practice.

Keywords Cytoskeleton, LINC complex, Mechanotransduction, Proliferation, Tissue remodeling, YAP

Background

Periodontal ligament (PDL) is highly specialized connective tissue between teeth and alveolar bone, which plays an important role in oral health. It not only protects and supports teeth, but also helps maintain the stability and normal function of oral structure [1]. The special position of PDL suggests periodontal ligament stem cells (PDLSCs) may be the preferred cell receptors in response to various mechanical stimuli, such as tension stress (TS), compressive stress and fluid shear stress [2–5]. These stimuli are transmitted into PDLSCs through mechanosensitive receptors, ion channels and focal adhesion domains, subsequently inducing cell proliferation, apoptosis and differentiation [6]. PDLSCs have recently been recognized as seed cells in tissue engineering, possessing the potential of self-renewal and regenerating damaged tissues and organs [7–9]. Recent studies have confirmed that PDLSCs can release neurotrophic factors and promote myelination and neuron regeneration [10]. In clinics, sufficient proliferation of PDLSCs is the premise for maintaining the integrity of PDL, promoting osteogenic differentiation, and keeping effective orthodontic tooth movement (OTM) [6, 7, 11]. However, in most cases, promoting cell proliferation is more challenging than inducing cell apoptosis [12]. Thus, developing effective methods to expand PDLSCs is essential.

Yes-associated protein (YAP) is a downstream effector of the Hippo pathway. Serving as a crucial regulatory factor in mechanical transduction [13], YAP can promote the transcription of downstream genes by interacting with members of the transcriptional enhanced associate domain (TEAD) family, significantly affecting organ development, tissue regeneration, tumorigenesis and metastasis [14, 15]. Typically, YAP shuttles between the cytoplasm and the nucleus. In certain conditions, such as sensing hard extracellular matrix or mechanical stimuli, YAP enters the nucleus to initiate downstream transcription [16]. Several studies have confirmed that YAP is widely involved in the fate regulation of PDLSCs under mechanical stimuli. Fluid shear stress can promote the proliferation of PDLSCs via the p38-AMOT-YAP axis [5]. LRP6 can regulate the osteogenic differentiation of PDLSCs in response to cyclic stretch stress through the F-actin/YAP cascade [3]. TS is one of the most frequently perceived mechanical forces of PDLSCs in vivo. However, it remains unclear whether TS can promote the proliferation of PDLSCs and whether YAP is involved. Furthermore, although we know the activation of YAP is not only related to the typical negative phosphorylation cascade of the Hippo pathway but also mechanical regulation [3, 5, 17, 18], the exact mechanism of YAP's entry into the nucleus induced by mechanical force is not fully understood.

In recent years, an increasing number of researchers have begun to focus on the linker of nucleoskeleton and cytoskeleton (LINC) complex at the nuclear envelope. The LINC complex consists of an outer nuclear envelope protein that contains the Klarsicht, ANC-1 and Syne Homology (KASH) domain, and an inner nuclear envelope protein that contains the Sad-1 and UNC-84 (SUN) domain. The two proteins are bound to each other in the perinuclear space. There are five types of Nesprin proteins with KASH domain (Nesprin1-4 and KASH5) and five types of SUN proteins (SUN1-5) in mammals, where SUN3-5 are specifically expressed only in sperm cells. This complex anchors the cytoskeletons on the cytoplasmic side and connects with the lamin on the nucleoplasm side [19–21], forming a continuous path for force transfer from the cytoskeletons to chromatin [22, 23]. Recently, many functions of the LINC complex have been confirmed, such as facilitating chromatin transcription, helping endothelial cell adhesion, and maintaining the progenitor state of basal keratinocytes [24–27]. However, the role of the LINC complex in mechanical signal transduction caused by TS, especially its interdependence with cytoskeletons, remains to be confirmed. In addition, mitochondria—the cellular energy factories—are often systematically transported to locations where energy is needed, providing the necessary ATP for various biological processes. Mitochondria also maintain complex connections with the cytoskeletons [28]. Nevertheless, the specific function of mitochondria under TS stimulus has not yet been understood.

This study aimed to explore the appropriate conditions for TS to promote the proliferation of PDLSCs, elucidate the relationship between YAP and PDLSCs proliferation, and focus on investigating the mechanism of YAP nuclear translocation under TS. We found that appropriate TS both in vitro and in vivo could induce the nuclear translocation of YAP, thus promoting cell proliferation. Cytoskeletons and, especially the cytoskeleton dynamics-dependent LINC complex, played important roles in TS-induced YAP nuclear translocation. These findings could provide theoretical evidence for seed cell expansion and for promoting healthy and effective OTM. Additionally, the mechanism may also apply to the nuclear translocation of other nuclear transcription factors under mechanical stress.

Methods

Cell culture

The extraction procedures of human PDLSCs in this study were approved by the Ethics Committee of Stomatological Hospital of Chongqing Medical University (No: 2023151) and conducted in accordance with the Declaration of Helsinki. Informed consent was obtained from the donors and/or their guardians before the tooth collection. Healthy premolars or third molars from young patients aged 12–25 years old, who were indicated for tooth extraction, were collected. The PDL from the middle third of the root was carefully scraped and cut up, then digested with 3 mg/mL collagenase I (C0130, Sigma-Aldrich, MO, USA) at 37 °C for 30 min. After centrifuging, the cells were cultured in a humidified atmosphere consisting of 95% air and 5% CO_2 at 37 °C. The culture medium used was α-minimum essential medium (α-MEM; SH30265.01, Hyclone, UT, USA) supplemented with 10% fetal bovine serum (FBS; S711-001S, Lonsera, Uruguay, USA) and 1% penicillin-streptomycin (SV30010, Invitrogen, CA, USA). Cells from passages 3 to 5 were utilized for subsequent experiments.

TS application in vitro

PDLSCs were seeded into the Bioflex culture plates (Flexcell, North Carolina, USA). The cyclic equiaxial TS (12% elongation, 0.5 Hz) was performed using the Flexcell® FX-5000 ™ Tension System (Flexcell, North Carolina, USA) to mimic orthodontic loading in vitro [29]. The duration of TS loading was either 6 h or 24 h. For the control group, cells were cultured under identical conditions but without the application of TS.

Chemicals and reagents

Cytochalasin D (CD; 0.2 μM, MedChemExpress, NJ, USA) was used to depolymerize F-actin, while Nocodazole (NO; 2 μM, Selleck, Texas, USA) was used for the depolymerization of microtubules. Oligomycin A (OA; 10 μM, Selleck, Texas, USA) was used to inhibit ATP synthase (mitochondrial respiratory chain complex V). The inhibitors were added to the cultured PDLSCs 30 min before the application of TS.

Cytoskeleton staining and mitochondria-related assays

To stain F-actin, Actin-Tracker Red-Rhodamine (C2207S, Beyotime, Shanghai, China) and Actin-Tracker Green-488 (C2201S, Beyotime, Shanghai, China) were utilized. Microtubules were stained using Tubulin-Tracker Green (C1051S, Beyotime, Shanghai, China). MitoTracker Green (C1048, Beyotime, Shanghai, China) and MitoTracker Red (M7512, Invitrogen, CA, USA) were used to stain total mitochondria, the JC-1 Kit (C2003S, Beyotime, Shanghai, China) was employed for mitochondrial membrane potential (MMP) assessment, and the ATP Assay Kit (S0027, Beyotime, Shanghai, China) was used for measuring cellular ATP content. All operations were performed according to the manufacturer's instructions. For ease of observing the cell fluorescence staining in this study, silicone membranes were cut from Bioflex culture plates carefully and transferred to Glass Bottom Cell Culture Dish (BS-20-GJM, Biosharp, China), then rapidly visualized and captured under the fluorescence microscope (EVOS, USA). The quantitative analysis was performed using ImageJ software (NIH, USA).

Transmission Electron Microscopy (TEM)

PDLSCs were collected and centrifuged at 1200 rpm for 10 min. The cell cluster at the bottom was fixed with 2.5% glutaraldehyde in 0.1 M sodium cacodylate buffer and was dehydrated with ethanol. Following polymerization, ultrathin sections of 50 nm were made with uranyl acetate and lead citrate staining. The nuclear pore and distribution of mitochondria were observed by a TEM (JEOL JEM-1400Plus, Tokyo, Japan). The quantitative analysis was performed using ImageJ software.

Flow cytometry

PDLSCs were dissociated into single cells using 0.25% trypsin (SH30042.01, Hyclone, UT, USA). They were then centrifuged twice in phosphate buffered saline (PBS; BL302A, Biosharp, China) at 1000 rpm for 5 min. Finally, the cells were resuspended in 500 μL PBS for apoptosis detection. For cycle detection, the cells were resuspended in 100 μL PBS with 500 μL of precooled 75% ethanol. Data was acquired using a flow cytometer (CytoFLEX, Beckman, USA) and analyzed with FlowJo software (version 10, USA). The proliferation index (PI) was calculated using the following equation [30]:

$$\mathrm{PI}\ (\%) = \left[\frac{(\mathrm{S} + \mathrm{G2/M})}{(\mathrm{G0/G1} + \mathrm{S} + \mathrm{G2/M})}\right] \times 100$$

Quantitative real-time polymerase chain reaction (qRT-PCR)

PDLSCs were washed twice with PBS. Total cellular RNA was extracted using the RNAiso Plus reagent (Takara, Japan). The cDNA was reverse transcribed by the PrimeScript ™ RT reagent Kit (Takara, Japan) in a 10 μL system. Subsequently, qRT-PCR was performed by the CFX96 Touch ™ system (Bio-Rad, Hercules, CA, USA) using TB Green® Premix Ex Taq ™ II (Takara, Japan). GAPDH was set as the internal control. The primer sequences of all the target genes are listed in Additional file 1: Table S1.

Protein extraction and western blotting

PDLSCs were washed twice with precooled PBS. Total cellular protein was extracted using RIPA lysis buffer (P0013B, Beyotime, Shanghai, China) with 1% PMSF (ST506, Beyotime, Shanghai, China). Nuclear and cytoplasmic proteins were extracted following the instructions of the Nuclear and Cytoplasmic Protein Extraction Kit (P0027, Beyotime, Shanghai, China). All protein extraction processes were performed on ice. Protein concentrations were determined by the BCA Protein Assay Kit (ZJ102, Epizyme Biotech, Shanghai, China). Proteins were separated by sodium dodecyl sulfate polyacrylamide gel electrophoresis (SDS-PAGE) using appropriate gels (Epizyme Biotech, Shanghai, China) and then transferred onto 0.2 μm polyvinylidene fluoride (PVDF) membranes (ISEQ00010, Millipore, MA, USA). The membranes were blocked by 5% skim milk at room temperature for 2 h and then incubated with the primary antibodies overnight at 4 °C. HRP-conjugated secondary antibodies were incubated with the membranes at room temperature for 1.5 h. The Enhanced Chemiluminescence Kit (SQ201, Epizyme Biotech, Shanghai, China) was used for detecting the target protein, and ImageJ software was used for quantification analysis. GAPDH served as the internal control for total cellular protein and cytoplasmic protein, and H3 was used as the internal control for nuclear protein. Details of the antibodies are provided in Additional file 1: Table S2.

Small interfering RNA (siRNA) transfection

The siRNA targeting YAP was designed and synthesized by OBiO Biotechnology Co., Ltd. (Shanghai, China). The siRNA sequences are detailed in Additional file 1: Table S3. The siRNA was transfected into PDLSCs using Lipo3000 transfection reagent (L3000015, ThermoFisher Scientific, USA), following the manufacturer's instructions. PDLSCs transfected with a negative control siRNA served as the control group (siCon), while the FAM-labeled negative control was utilized to evaluate the siRNA transfection efficiency. The knockdown efficiency was confirmed by qRT-PCR and western blotting analysis.

Adenovirus construction and transfection

The adenovirus was designed and constructed as described previously [23, 26, 31] by OBiO Biotechnology Co., Ltd. (Shanghai, China). DNKASH, a dominant negative protein composed of the KASH domain of Nesprin1, was combined with mCherry, a red fluorescence protein, to create ADV-mCherry-DNKASH (sequence from addgene plasmid 125553). ADV-mCherry, containing only mCherry, served as a control. Adenovirus transfection was carried out according to the manufacturer's instructions. The optimal multiplicity of infection (MOI) was determined by observing the transfection efficiency through fluorescence imaging. The TS loading was performed after adenovirus transfection for 48 h.

Osteogenic induction and alkaline phosphatase (ALP) staining

PDLSCs were cultured in α-MEM, either with or without osteogenic induction ingredients (dexamethasone (100 nM), β-glycerophosphate (10 mM) and ascorbic acid (50 μg/ml) (Sigma-Aldrich, MO, USA)) for different groups. The medium was changed every 2 days. For the force loading group, TS was applied for 12 h every 12 h, lasting for 7 days. After 7 days, qRT-PCR was utilized to detect the expression of osteogenic-related genes, and ALP staining was performed using the BCIP/NBT Alkaline Phosphatase Staining Kit (C3206, Beyotime, Shanghai, China) according to the manufacturer's instructions.

Animal model establishment

All animal experiments were approved by the Ethics Committee of Stomatological Hospital of Chongqing Medical University (No: 2023151). A total of 45 healthy Sprague-Dawley (SD) rats (male, 6-week-old, 200±20 g) were purchased from the Animal Center of Chongqing Medical University (Chongqing, China). All the rats were housed in the SPF-grade rat foster room of Chongqing Key Laboratory of Oral Diseases, with a 12-hour day/night cycle. The rats were allowed to eat and drink freely. All rat cages were placed on the same rack. Following 3 days of adaptive feeding, the rats were randomly assigned to different groups by the first investigator (the only person aware of the group allocation and responsible for managing the entire experiments, yet did not perform any operations), with five rats in each group. Random numbers were generated using the standard=RAND () function in Microsoft Excel. The sample size was determined based on previous research [3, 32]. The second investigator was responsible for anesthesia and administering. Specifically, the rats were weighed first. A 2% pentobarbital sodium solution was prepared using physiological saline, then the intraperitoneal injection was administered to the rats at a dose of 0.2 mL/100 g weight; the anesthetic effect was achieved in about 10 min. The

model constructions were completed by the third investigator. The rats were finally included in the analysis only if they maintained a normal diet, were in a good mental state, showed no abnormal behavior, and exhibited no illness or fatalities. Otherwise, they were excluded.

To construct the OTM model, the nickel-titanium tension spring (0.010 inch × 6 mm, Superline, Shenzhen, China) delivered a force of 30 g measured by a spring dynamometer (AOSU, China), was ligated between the maxillary left first molar and incisor for each rat. The force was applied for 3, 7 and 14 days (5 rats per group). The maxillary right dentition served as a control. The model was checked daily, and any loose springs were replaced promptly. For intervention experiments, CsCl purified adenovirus was purchased from OBiO Biotechnology Co., Ltd. (Shanghai, China). The adenovirus used in rats had the same design and function as that used in cell experiments, but it was more suitable for in vivo research after CsCl purification. The group injected with the target adenovirus formed a control with the group injected with the control adenovirus. The local injection method and dose for rats were done as described previously by the second investigator [33, 34]. ADV-mCherry-DNKASH (the target adenovirus, denoted as ADV-DNKASH, for distinction from the in vitro adenovirus) or ADV-mCherry (the control adenovirus, denoted as ADV-Con for distinction) was locally injected at four sites around the maxillary left first molar using a microsyringe (25 μL syringe, Hamilton Company, Nevada, USA), including the mesiobuccal, distobuccal, mesiopalatal and distopalatal gingival sulcus, and the total injection dose for each rat was 1.0E+9 PFU. The OTM model was established 3 days post adenovirus injection, with the 30 g-force application periods being 3, 7 and 14 days (5 rats per group). During the experiment, all rats met the inclusion criteria. Therefore, all rat samples were eventually harvested after euthanasia. The euthanasia procedure was carried out as follows: The euthanasia chamber (transparent, 10 L) was cleaned first, then the rats were placed inside and the chamber was locked tightly. The compressed CO_2 gas cylinder was opened, and the CO_2 gas flowmeter was adjusted to fill CO_2 at a constant speed of 5–6 L/minute, equivalent to displacing 50–60% of the chamber volume per minute. After the rats stopped breathing, the CO_2 continued to flow for at least 1 min. After the CO_2 gas flowmeter was turned off, another 2 min of observation was kept to fully confirm the death of the rats (such as cessation of heartbeat and breathing, stiffness of the body, and dilation of the pupils). Subsequently, the CO_2 gas cylinder was closed, the rats were taken out, and the euthanasia chamber was cleaned. After the samples were prepared successfully, alveolar bone height, tooth movement distance and periodontal tissue remodeling were assessed.

Micro Computed Tomography (micro-CT)

The maxillary bones (with teeth) of rats were fixed in 4% paraformaldehyde (BL539A, Biosharp, China) for 48 h and then washed overnight with running water. Subsequently, the maxillary bones were scanned with a micro-CT system (VivaCT40, SCANCO, Switzerland) with a voxel resolution of 17.5 μm. The three-dimensional (3D) reconstruction and X-ray images were acquired by Mimics software (version 21.0, Belgium) to estimate the alveolar bone height and the tooth movement distance (the anterior-posterior distance between the first molar crown and the second molar crown).

Hematoxylin and Eosin (HE) staining

After decalcification in 20% ethylenediaminetetraacetic acid (EDTA; V900081, Sigma-Aldrich, MO, USA) for 1.5 months, the maxillary bones (with teeth) were embedded in paraffin (39601095, Leica, Wetzlar, Germany) and cut into 5 μm sections. HE staining was conducted using the HE Staining Kit (G1120, Solarbio, Beijing, China) according to the manufacturer's instructions.

Immunofluorescence staining

For cell immunofluorescence staining, PDLSCs were fixed with 4% paraformaldehyde for 15 min at room temperature. Then 0.5% Triton X-100 (P1080, Solarbio, Beijing, China) was used for permeating the cytomembrane, and 5% goat serum (C-0005, Bioss, Beijing, China) was used for blocking the cells. Next, the cells were incubated with primary antibodies overnight at 4 °C, followed by incubation with fluorescent secondary antibodies for 1 h at room temperature. Nuclei were stained with DAPI (P0131, Beyotime, Shanghai, China). Finally, the cells were rapidly visualized and imaged under the fluorescence microscope (EVOS, USA). For tissue immunofluorescence staining, after dewaxing with xylene and rehydrating with gradient ethanol, the tissue sections were placed in sodium citrate antigen repair solution (P0083, Beyotime, Shanghai, China) for 20 min at 95℃. The subsequent steps were identical to those for cell immunofluorescence staining. Finally, the tissue was quickly observed and imaged under the fluorescence microscope (Zeiss, Germany). The quantitative analysis was performed using ImageJ software. Details of the antibodies are provided in Additional file 1: Table S2.

Statistical analysis

GraphPad Prism software (version 9.0, USA) was used to analyze and graph the data. An unpaired Student's t-test was conducted when two independent groups were analyzed. For multiple comparisons, the one-way analysis of variance (ANOVA) was performed. The normality and homogeneity of the data were checked before performing the one-way ANOVA, which was followed

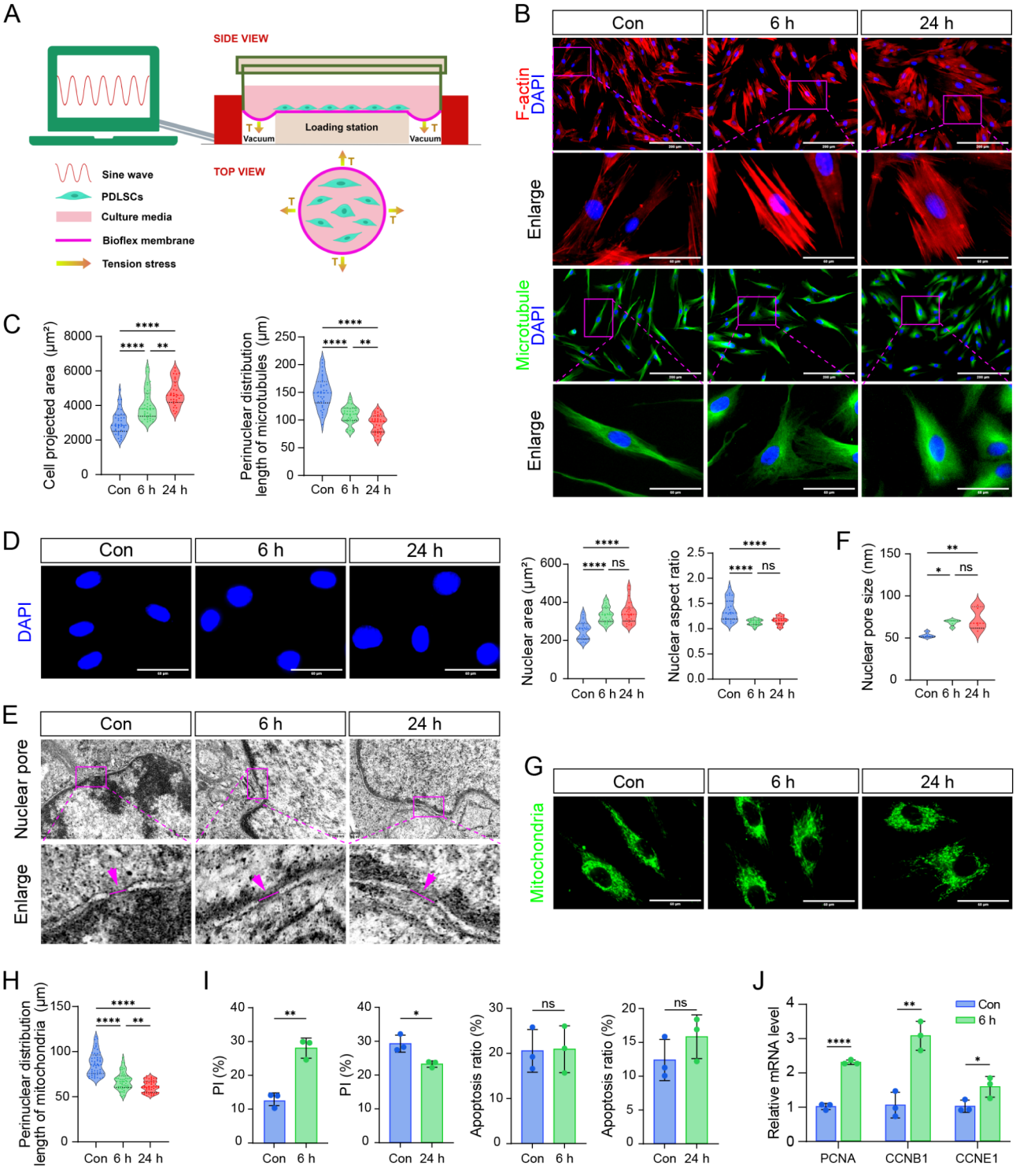

Fig. 1 (See legend on next page.)

by Tukey's post hoc test. The results were presented as means ± standard deviations of at least three independent experiments. $P<0.05$ was considered a significant difference (* $P<0.05$, ** $P<0.01$, *** $P<0.001$, **** $P<0.0001$, and "ns" indicating comparisons did not have statistical significance).

(See figure on previous page.)

Fig. 1 TS led to rearrangement in PDLSCs morphology and affected cell life activities. **A** Schematic diagram of the TS loading system in vitro. **B** Fluorescence staining of cytoskeletons after TS application. Scale bars = 200 μm in the first and third rows. The second and fourth rows showed enlarged images of the upper magenta boxes, scale bars = 50 μm. **C** Quantitative analysis of the cell projected area corresponding to F-actin (n = 38, 38, 30 roi, respectively) and the perinuclear distribution length of microtubules (n = 35 roi per condition) after TS application. The perinuclear distribution length of microtubules was defined as the longest straight-line distance between two boundary points of microtubules passing through the nucleus. **D** Fluorescence staining of the nucleus and quantitative analysis of the nuclear area and nuclear aspect ratio after TS application (n = 25 roi per condition). Scale bars = 50 μm. **E** TEM images of the nuclear pores after TS application. Scale bars = 200 nm. The lower row showed enlarged images of the upper magenta boxes, with the magenta arrows and lines indicating the nuclear pores, scale bars = 40 nm. **F** Quantitative analysis of nuclear pore size after TS application (n = 5 roi per condition). **G** Fluorescence staining of mitochondria after TS application. Scale bars = 50 μm. **H** Quantitative analysis of the perinuclear distribution length of mitochondria after TS application (n = 50 roi per condition). The perinuclear distribution length of mitochondria was defined as the longest straight-line distance between two boundary points of mitochondria passing through the nucleus. **I** The PI and apoptosis ratio after TS application for 6 h or 24 h. **J** The mRNA level of proliferation-related genes after TS application for 6 h

Results

TS led to rearrangement in PDLSCs morphology and affected cell life activities

PDLSCs were subjected to a tension system for either 6 h or 24 h in vitro (Fig. 1A). Under normal conditions, the cytoskeletons in PDLSCs were arranged in a regular pattern. F-actin was mainly distributed inside the cell membrane, whereas microtubules were primarily located around the nucleus and radiated towards the cytoplasm (Additional file 2: Fig. S1). After applying TS, the cell morphology was significantly remodeled. F-actin became wider and denser, and the cell projected area increased significantly. The distribution of microtubules shifted from a long spindle shape to a more extensive and uniform distribution around the nucleus, and the perinuclear distribution length of microtubules decreased significantly (Fig. 1B, C). The nuclear area expanded, but the aspect ratio decreased (Fig. 1D). TEM showed that TS enlarged the size of the nuclear pore (Fig. 1E, F). Interestingly, the distribution pattern of mitochondria resembled that of microtubules, and the stress significantly reduced the length of mitochondrial perinuclear distribution (Fig. 1G, H). Flow cytometry analysis revealed that applying TS for 6 h promoted cell proliferation, but continuous application of TS for 24 h inhibited cell proliferation; neither 6 h or 24 h of TS application significantly induced cell apoptosis (Fig. 1I). Further qRT-PCR confirmed that applying TS for 6 h promoted the expression of proliferation-related genes in PDLSCs (Fig. 1J). Overall, all of the morphological indices showed significant changes after TS application for 6 h, with cell proliferation being active. Therefore, the 6-hour TS application was selected for subsequent studies.

TS triggered YAP nuclear translocation in PDLSCs and PDL tissue and promoted cell proliferation

We explored the response pattern of YAP, a transcription factor sensitive to mechanical stimuli, in PDLSCs and PDL tissue. The in vitro results indicated that TS promoted the mRNA expression of YAP (Fig. 2A) and YAP target genes (Additional file 2: Fig. S2A), yet had little effect on the total protein expression of YAP within 6 h (Fig. 2B). Immunofluorescence staining and western blotting results showed that TS significantly promoted the nuclear translocation of YAP (Fig. 2C, D). When YAP was knocked down by siRNA (Additional file 2: Fig. S2B-D), the TS-induced proliferation of PDLSCs was significantly downregulated, and the application of TS no longer promoted the expression of proliferation-related genes (Fig. 2E). These findings demonstrated that TS promoted the nuclear translocation of YAP, subsequently promoting the proliferation of PDLSCs. Unsurprisingly, TS was also found to encourage osteogenic differentiation of PDLSCs (Additional file 2: Fig. S3). Furthermore, we established the rat OTM model (Additional file 2: Fig. S4). The micro-CT analysis confirmed that the continuous force loading of 30 g for 14 days was appropriate. There was no significant loss of alveolar bone height (Fig. 2F). The distance of OTM increased with time (Fig. 2G). HE staining revealed that within 14 days, the PDL on the tension side gradually reverted to its normal width from rapid stretching, and similarly, the PDL on the pressure side also returned to its normal width from rapid compression. By the 14th day, periodontal tissue had remodeled completely, with bilateral periodontal fibers appearing continuous and dense (Fig. 2H). Immunofluorescence staining of the tension side PDL tissue revealed that YAP nuclear translocation occurred on the 3rd day following force loading, peaking on the 7th day (Fig. 2I and Additional file 2: Fig. S5A). Similarly, the proliferating cell nuclear antigen (PCNA)-positive cells emerged on the 3rd day and reached the peak on the 7th day (Fig. 2J and Additional file 2: Fig. S5B).

F-actin dynamics participated in TS-induced YAP nuclear translocation in PDLSCs

As mentioned above, applying TS for 6 h led to a dramatic reconstruction of the cytoskeletons in PDLSCs. This led us to speculate that the cytoskeleton changes might be linked to the TS-induced YAP nuclear translocation. To test this hypothesis, we depolymerized microtubules with NO or depolymerized F-actin with CD for subsequent research. Fluorescence staining confirmed that the depolymerization of one cytoskeleton did not affect the

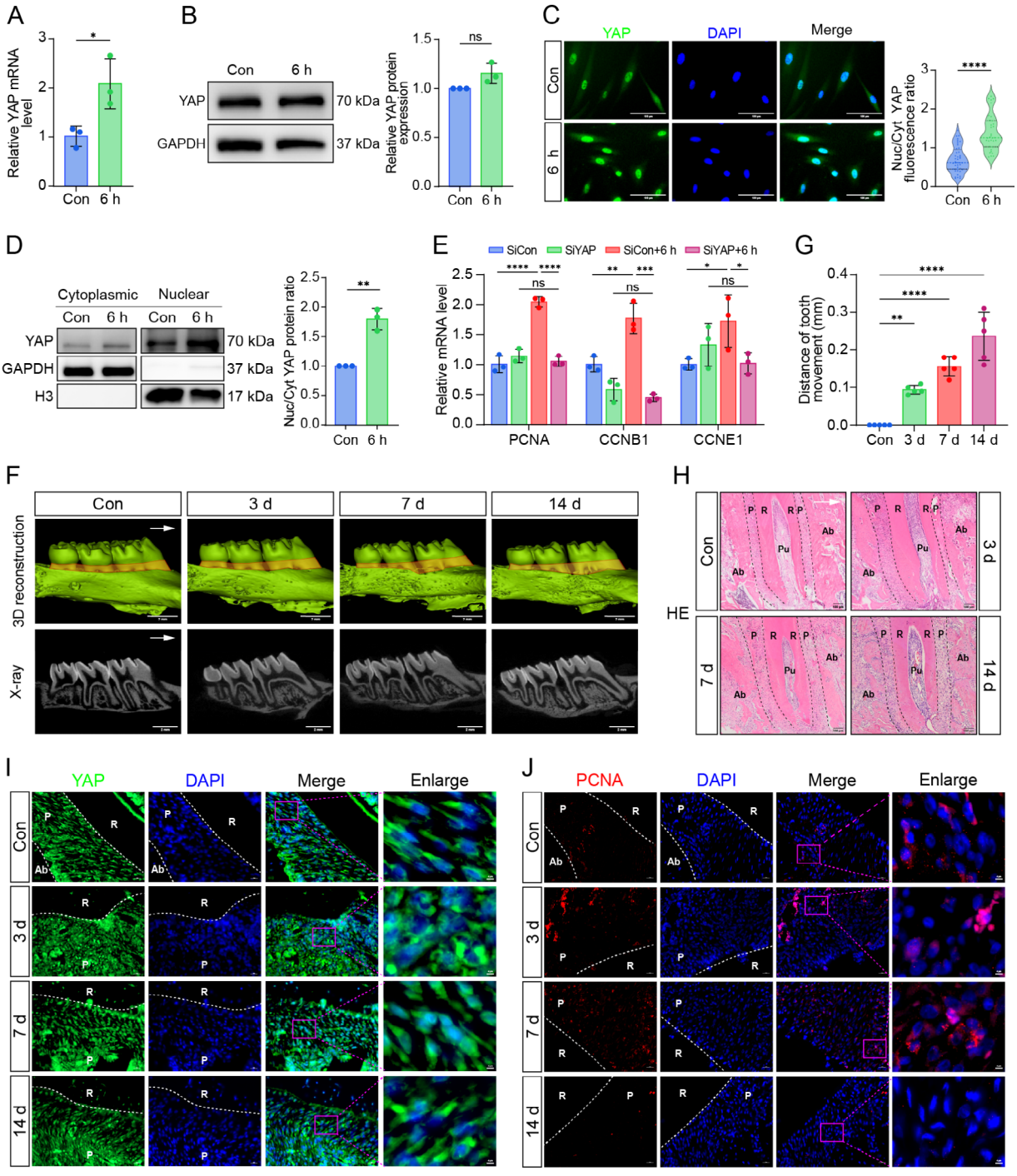

Fig. 2 TS triggered YAP nuclear translocation in PDLSCs and PDL tissue and promoted cell proliferation. **A** The mRNA level of YAP after TS application. **B** The protein expression of YAP and quantitative analysis after TS application. **C** Immunofluorescence staining of YAP and quantitative analysis of nuclear/cytoplasmic YAP fluorescence ratio after TS application ($n = 44$, 33 roi, respectively). Scale bars = 100 μm. **D** The nuclear and cytoplasmic protein expression of YAP and quantitative analysis after TS application. **E** The mRNA level of proliferation-related genes after siRNA transfection. **F** The representative 3D reconstruction and X-ray images of rat maxillary bones after force loading 0 day (Con), 3 days, 7 days and 14 days. The arrow indicated the direction of tooth movement. Scale bars = 2 mm. **G** Quantitative analysis of tooth movement distance in rats ($n = 5$). **H** Representative HE staining of the distal buccal root of the maxillary first molar in rats. The arrow indicated the direction of tooth movement, and dotted lines marked the boundary of PDL. Ab, Alveolar bone; P, PDL; R, Root; Pu, Pulp. Scale bars = 100 μm. **I** YAP immunofluorescence staining of the tension side PDL tissue in rats. Scale bars = 20 μm. The last column showed enlarged images of the left magenta boxes. Ab, Alveolar bone; P, PDL; R, Root. Scale bars = 4 μm. **J** PCNA immunofluorescence staining of the tension side PDL tissue in rats. Scale bars = 20 μm. The last column showed enlarged images of the left magenta boxes. Ab, Alveolar bone; P, PDL; R, Root. Scale bars = 4 μm

arrangement of the other cytoskeleton (Fig. 3A). Further findings revealed that although the depolymerization of the two cytoskeletons did not alter YAP mRNA level under TS (Fig. 3B), the depolymerization of F-actin significantly inhibited YAP nuclear localization (Fig. 3C-F), as well as the mRNA expression of proliferation-related genes (Fig. 3G). Interestingly, we noticed that TS application somewhat upregulated F-actin both inside and outside the nucleus, whereas the addition of CD downregulated F-actin both in the cytoplasm and nucleus, although these differences were not significant (Fig. 3H). These results fully confirmed that F-actin dynamics participated in TS-induced YAP nuclear translocation in PDLSCs. In addition, we observed that the depolymerization of F-actin significantly reduced the nuclear area and increased the nuclear aspect ratio (Fig. 3I). This indicated that the nuclear morphology was regulated by F-actin dynamics and was closely related to YAP nuclear translocation.

The F-actin dynamics-dependent LINC complex was indispensable for TS-induced YAP nuclear translocation in PDLSCs

It has been established that F-actin dynamics participated in TS-induced YAP nuclear translocation and affected the nuclear morphology of PDLSCs. Considering that the LINC complex serves as an important bridge connecting the cytoskeleton and the nucleus, our research shifted focus to this complex. We discovered that TS significantly upregulated mRNA level of Nesprin1 and Nesprin2, but had little effect on Nesprin3 and Nesprin4 (Fig. 4A). Also, TS promoted the mRNA expression of SUN1 and SUN2 (Additional file 2: Fig. S6). Due to the similar expression pattern after TS application and the homology between Nesprin1 and Nesprin2, we chose Nesprin1 for further research. The addition of CD significantly decreased the mRNA and protein expression of Nesprin1 under TS, while NO had a negligible impact on it (Fig. 4B, C). Subsequently, we transfected PDLSCs with adenovirus (Additional file 2: Fig. S7). Immunofluorescence staining showed that ADV-mCherry-DNKASH prevented the localization of Nesprin1 on the nuclear envelope, which meant the LINC complex was successfully disrupted, while ADV-mCherry did not alter Nesprin1's localization (Fig. 4D). Subsequent immunofluorescence staining and western blotting results showed that TS-induced YAP nuclear translocation in ADV-mCherry-DNKASH-transfected PDLSCs was significantly inhibited for the disruption of the LINC complex (Fig. 4E-H). Correspondingly, the mRNA level of proliferation-related genes under TS was significantly downregulated following the disruption of the LINC complex (Fig. 4I). These findings unequivocally confirmed the indispensable role the LINC complex played in TS-induced YAP nuclear translocation, highlighting its dependence on F-actin dynamics.

The disrupted LINC complex prevented TS-induced YAP nuclear translocation in PDL tissue and hindered tooth movement

To further elucidate the essential role of the LINC complex for YAP nuclear translocation in vivo, we administered local injections of adenovirus to rats and subsequently established OTM models (Fig. 5A). HE staining confirmed that the adenovirus had no adverse effects on the vital organs of the rats, including the heart, liver, spleen, lung and kidney (Additional file 2: Fig. S8A). The 3D reconstruction and X-ray images indicated no significant loss in the height of alveolar bone between the groups within 14 days (Fig. 5B). While tooth movement distances in the ADV-Con groups gradually increased over time, the ADV-DNKASH groups exhibited small differences between adjacent time points. Notably, on days 7 and 14, tooth movement distances in the ADV-DNKASH groups were significantly less than those observed in the ADV-Con groups (Fig. 5C). The HE staining of periodontal tissue of the first molar revealed that in the ADV-Con groups, normal tissue remodeling occurred, similar to what was observed without adenovirus injection (Fig. 2H). Conversely, in the ADV-DNKASH groups, bilateral periodontal tissues failed to undergo normal remodeling. On the tension side, the PDL remained stretched, with periodontal fibers appearing loose and discontinuous. On the pressure side, the PDL remained compressed, and periodontal fibers showed signs of discontinuity and local necrosis (Fig. 5D). Immunofluorescence staining of the tension side PDL tissue revealed obvious YAP nuclear translocation in the ADV-Con groups on the 3rd and 7th days, peaking on the 7th day. By contrast, the ADV-DNKASH groups showed no evident YAP nuclear translocation at any time point (Fig. 5E). The average nuclear YAP fluorescence intensity in the ADV-DNKASH groups was significantly lower than that in the control groups, except on the 14th day (Additional file 2: Fig. S8B). The pattern observed in PCNA immunofluorescence staining of the tension side PDL tissue was similar to that of YAP (Fig. 5F), where the number of PCNA-positive cells in the ADV-DNKASH groups was significantly lower than that in the control groups on the 3rd and 7th days (Additional file 2: Fig. S8C). These findings conclusively demonstrated that disrupting the LINC complex significantly inhibited TS-induced YAP nuclear translocation in PDL tissue, subsequently inhibiting cell proliferation, affecting normal periodontal tissue remodeling, and hindering tooth movement.

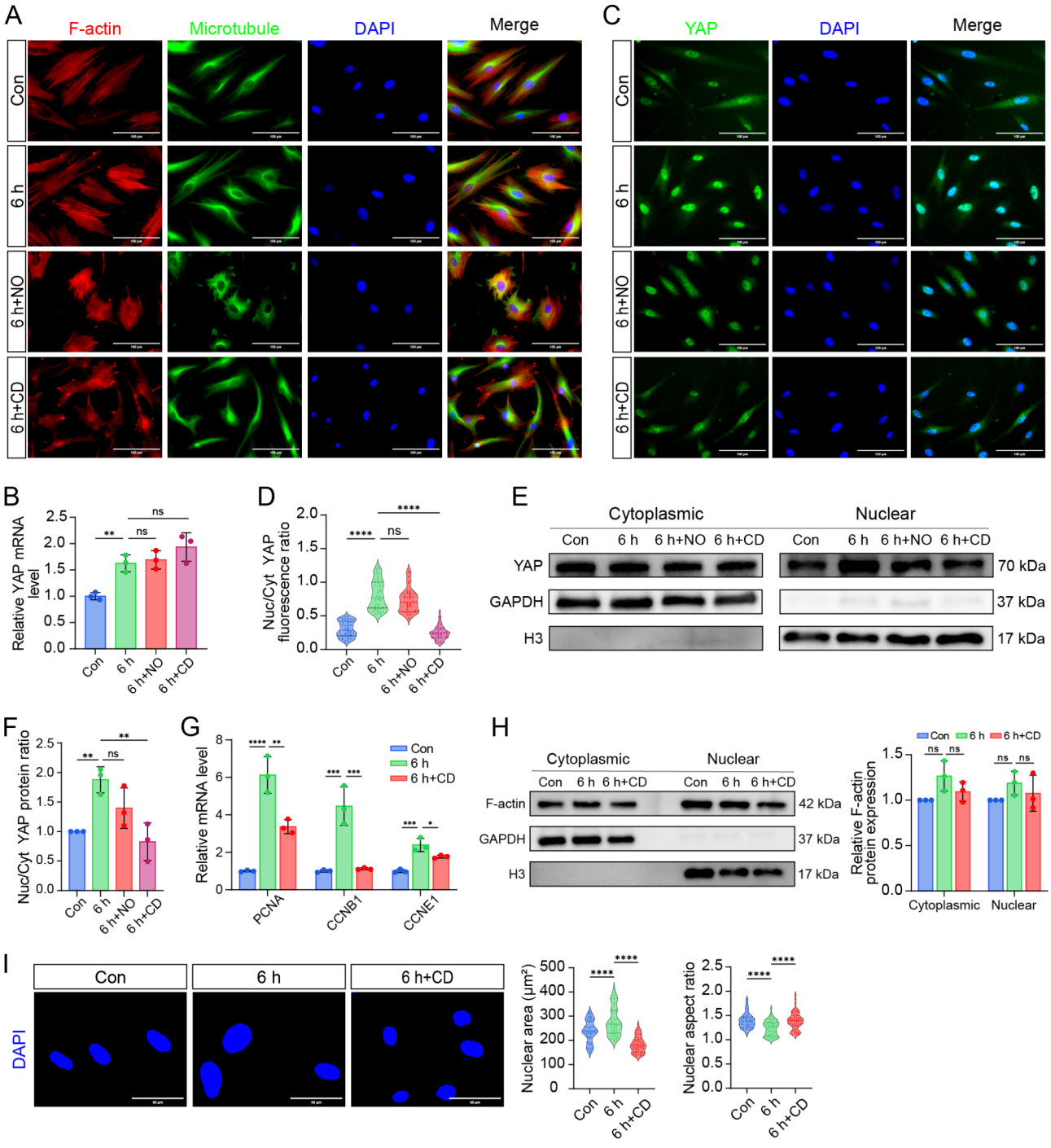

Fig. 3 F-actin dynamics participated in TS-induced YAP nuclear translocation in PDLSCs. **A** Fluorescence staining of cytoskeletons after adding cytoskeleton inhibitors. Scale bars = 100 μm. **B** The mRNA level of YAP after adding cytoskeleton inhibitors. **C** The immunofluorescence staining of YAP after adding cytoskeleton inhibitors. Scale bars = 100 μm. **D** Quantitative analysis of nuclear/cytoplasmic YAP fluorescence ratio after adding cytoskeleton inhibitors (n = 45, 45, 36, 45 roi, respectively). **E**, **F** The nuclear and cytoplasmic protein expression of YAP and quantitative analysis after adding cytoskeleton inhibitors. **G** The mRNA level of proliferation-related genes after adding F-actin inhibitor. **H** The nuclear and cytoplasmic protein expression of F-actin and quantitative analysis after adding F-actin inhibitor. **I** Nuclear fluorescence staining and quantitative analysis of nuclear area and nuclear aspect ratio after adding F-actin inhibitor (n = 55 roi per condition). Scale bars = 50 μm

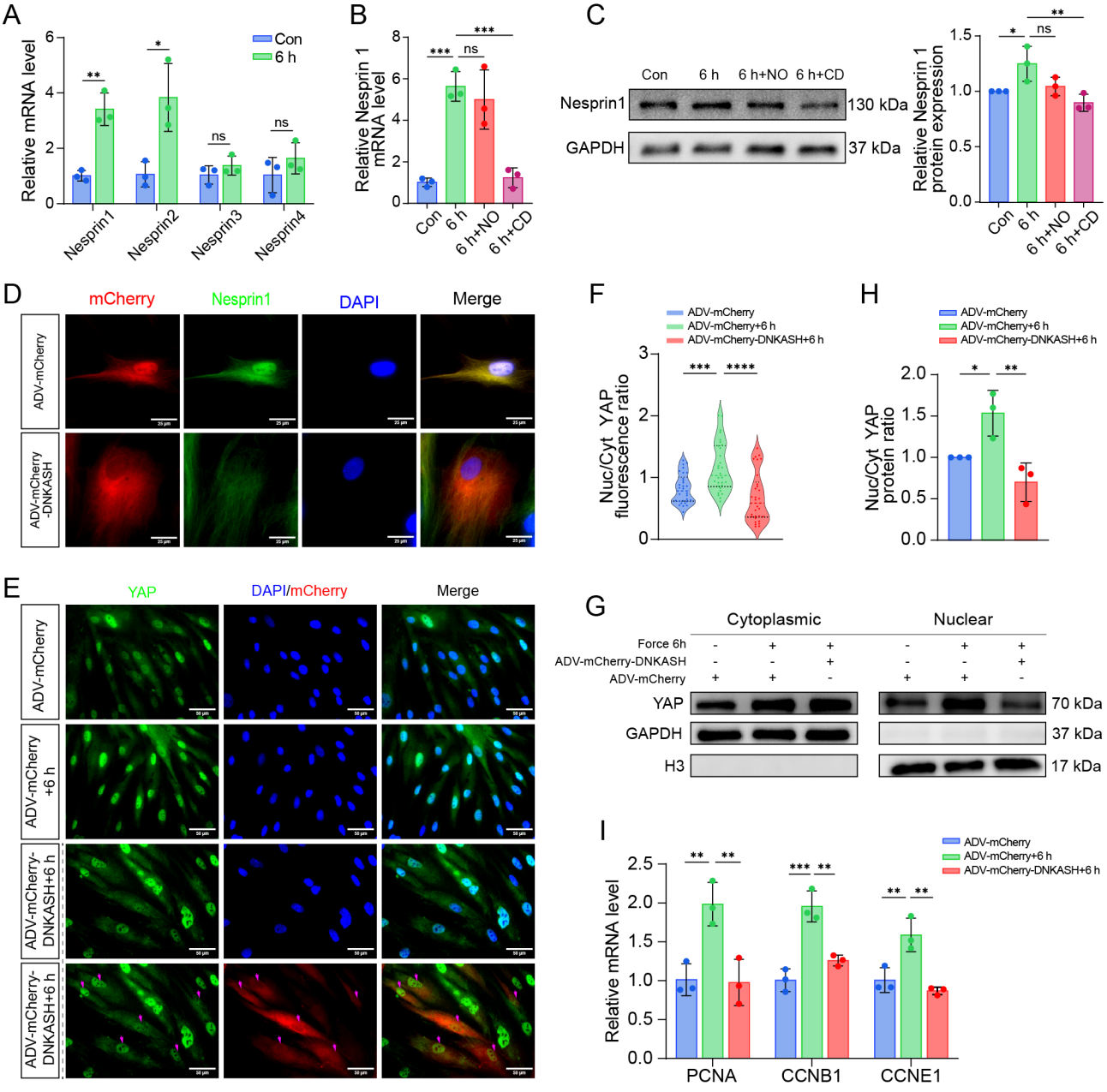

Fig. 4 The F-actin dynamics-dependent LINC complex was indispensable for TS-induced YAP nuclear translocation in PDLSCs. **A** The mRNA level of Nesprin1-4 after TS application. **B** The mRNA level of Nesprin1 after adding cytoskeleton inhibitors. **C** The protein expression of Nesprin1 and quantitative analysis after adding cytoskeleton inhibitors. **D** Immunofluorescence staining showed Nesprin1's nuclear envelope localization after adenovirus transfection. The mCherry was self-fluorescence of adenovirus. Scale bars = 25 μm. **E** Immunofluorescence staining of YAP after adenovirus transfection. The lowest row showed the cells with restricted YAP nuclear translocation were just the cells whose LINC complex was destroyed (the magenta arrows indicated). Scale bars = 50 μm. **F** Quantitative analysis of nuclear/cytoplasmic YAP fluorescence ratio after adenovirus transfection ($n = 30$ roi per condition). **G**, **H** The nuclear and cytoplasmic protein expression of YAP and quantitative analysis after adenovirus transfection. **I** The mRNA level of proliferation-related genes after adenovirus transfection

TS enhanced mitochondrial dynamics to provide ATP for YAP nuclear translocation in PDLSCs

Our above findings indicated that TS induced the repositioning of mitochondria around the nucleus. Further investigation demonstrated a close positional correlation between mitochondria and microtubules, as evidenced by fluorescence co-localization staining (Additional file 2: Fig. S9). TS promoted the perinuclear aggregation of mitochondria, and the addition of NO resulted in a scattered distribution of mitochondria (Fig. 6A), suggesting that TS-induced mitochondrial repositioning was triggered by microtubule remodeling. TEM further

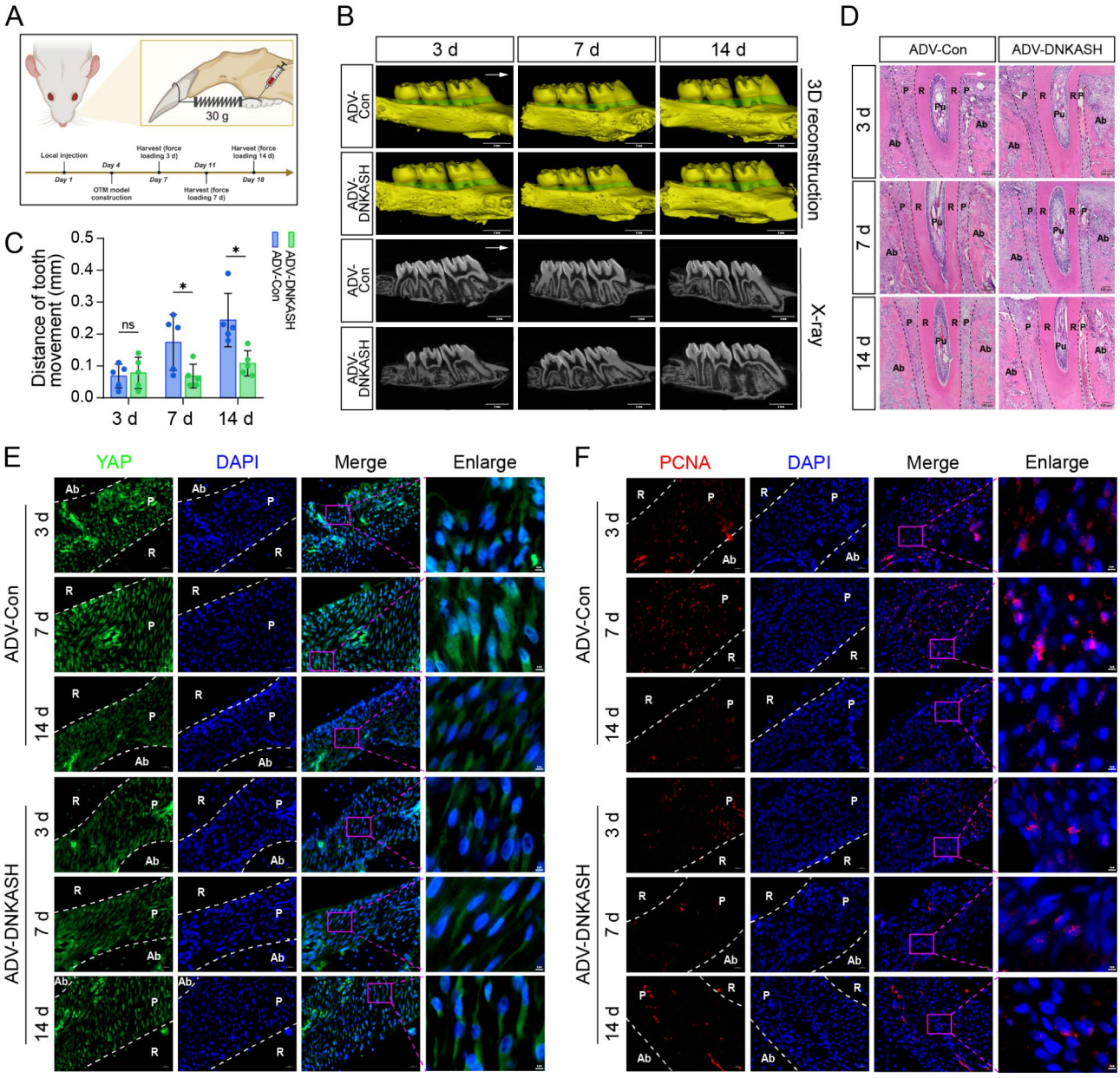

Fig. 5 The disrupted LINC complex prevented TS-induced YAP nuclear translocation in PDL tissue and hindered tooth movement. **A** Schematic diagram of adenovirus local injection and rat OTM model construction. **B** The representative 3D reconstruction and X-ray images of rat maxillary bones after force loading 3 days, 7 days and 14 days. The arrow indicated the direction of tooth movement. Scale bars = 2 mm. **C** Quantitative analysis of tooth movement distance in each group of rats ($n = 5$). **D** Representative HE staining of the distal buccal root of the maxillary first molar in each group of rats. The arrow indicated the direction of tooth movement, and dotted lines marked the boundary of PDL. Ab, Alveolar bone; P, PDL; R, Root; Pu, Pulp. Scale bars = 100 μm. **E** YAP immunofluorescence staining of the tension side PDL tissue in each group of rats. Scale bars = 20 μm. The last column showed enlarged images of the left magenta boxes. Ab, Alveolar bone; P, PDL; R, Root. Scale bars = 4 μm. **F** PCNA immunofluorescence staining of the tension side PDL tissue in each group of rats. Scale bars = 20 μm. The last column showed enlarged images of the left magenta boxes. Ab, Alveolar bone; P, PDL; R, Root. Scale bars = 4 μm

confirmed the perinuclear aggregation of mitochondria after TS application (Fig. 6B). At the same time, TS not only enhanced MMP (Fig. 6C, D) but also enhanced mitochondrial biogenesis, as well as mitochondrial fission and fusion dynamics (Fig. 6E). Given mitochondria's role as cellular energy generators, we hypothesized that these changes prepared mitochondria to supply energy for YAP nuclear translocation. This hypothesis was supported by the significant increase of ATP level in PDLSCs after TS application (Fig. 6F). Upon employing OA, an ATP synthase inhibitor, to inhibit ATP production under TS (Fig. 6G), we observed a notable limitation in TS-induced YAP nuclear entry (Fig. 6H, I and Additional file 2: Fig. S10A), and the corresponding decrease in the

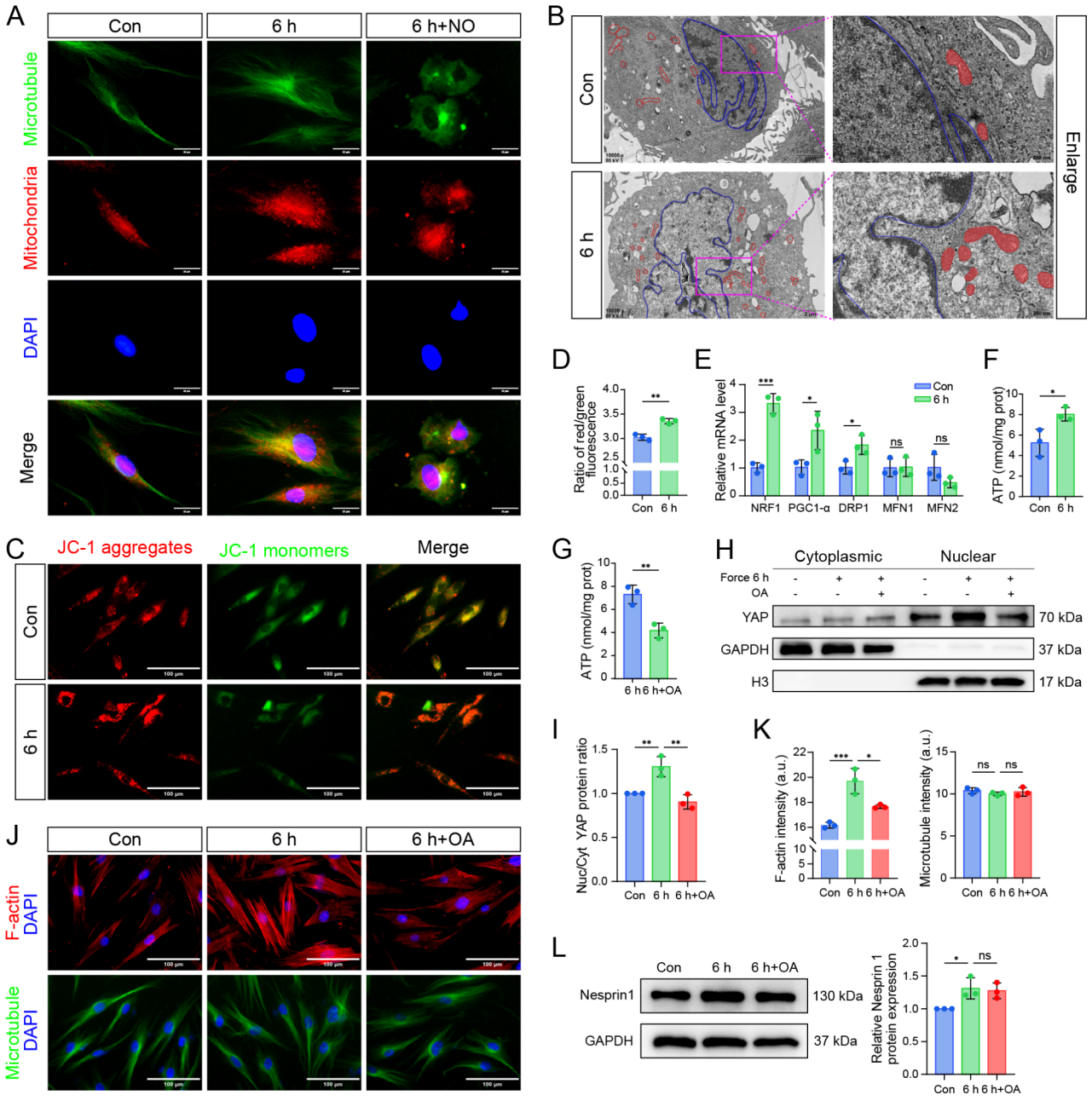

Fig. 6 TS enhanced mitochondrial dynamics to provide ATP for YAP nuclear translocation in PDLSCs. **A** Fluorescence co-localization staining of mitochondria and microtubules after adding microtubule inhibitor. Scale bars = 25 μm. **B** TEM showed the positional relationship of mitochondria and nucleus after TS application. The blue line depicted the nucleus outline and the red line depicted the mitochondria outline. Scale bars = 2 μm. The right column showed enlarged images of the left magenta boxes and the red shadow highlighted the mitochondria, scale bars = 200 nm. **C** JC-1 fluorescence staining after TS application. Scale bars = 100 μm. **D** Quantitative analysis of JC-1 fluorescence staining after TS application. **E** The mRNA level of mitochondrial biogenesis-related genes (NRF1, PGC1-α), mitochondrial fission-related gene (DRP1) and mitochondrial fusion-related genes (MFN1, MFN2) after TS application. **F** ATP content in PDLSCs after TS application. **G** ATP content in PDLSCs after adding ATP synthase inhibitor. **H**, **I** The nuclear and cytoplasmic protein expression of YAP and quantitative analysis after adding ATP synthase inhibitor. **J** Fluorescence staining of cytoskeletons after adding ATP synthase inhibitor. Scale bars = 100 μm. **K** Fluorescence intensity analysis of cytoskeletons after adding ATP synthase inhibitor. **L** The protein expression of Nesprin1 and quantitative analysis after adding ATP synthase inhibitor

expression of proliferation-related genes (Additional file 2: Fig. S10B), which further validated our hypothesis. Interestingly, inhibiting cellular ATP synthesis with OA significantly reduced the intensity of F-actin under TS, whereas microtubule intensity appeared unaffected (Fig. 6J, K). Besides, adding OA had little effect on the mRNA and protein expression of Nesprin1 (Fig. 6L and Additional file 2: Fig. S10C). These findings suggested

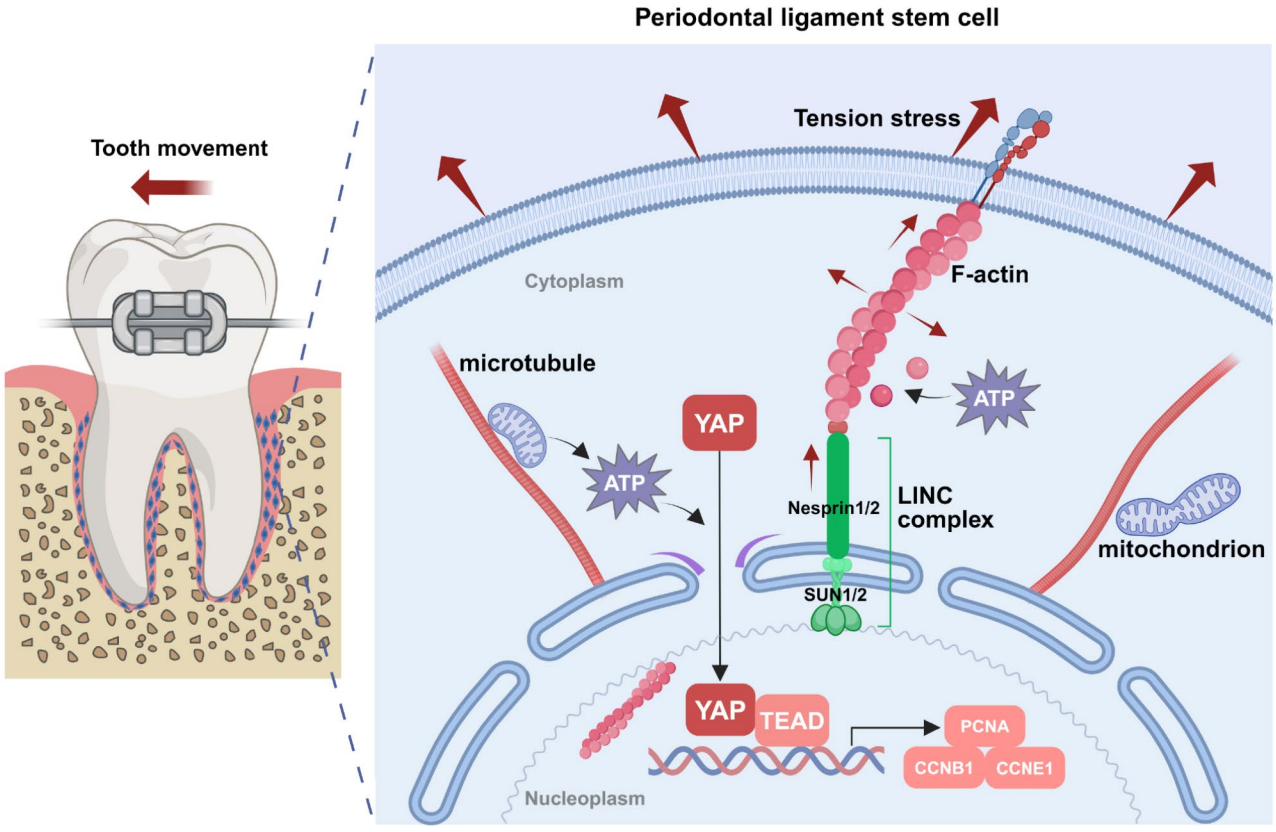

Fig. 7 Mechanism diagram. During the OTM process, PDLSCs on the tension side received continuous TS stimulus, which enhanced the polymerization and stretching of F-actin and then upregulated the expression of the LINC complex, thus strengthening the pull on the nuclear envelope, enlarging the nuclear pore and facilitating YAP's entry into the nucleus. At the same time, the mitochondria were activated and moved towards the nucleus along the reconstructed microtubules under the stress state, producing ATP to assist YAP nuclear translocation and to drive F-actin polymerization to a certain extent. YAP further promoted the expression of downstream proliferation-related genes after entering the nucleus, thus promoting cell proliferation and finally leading to effective tooth movement

that the active mitochondrial dynamics enhanced by TS not only supplied ATP for YAP nuclear translocation but also supported the polymerization of F-actin to a certain extent.

Discussion

PDLSCs were first discovered by Professor Seo's team in 2004 [35]. Since then, numerous studies have confirmed that PDLSCs possess strong potential for self-renewal and multi-directional differentiation, exhibiting broad therapeutic prospects in tissue regeneration [7–10]. However, the rarity of PDLSCs has hindered their further application [5]. TS is one of the most commonly perceived mechanical stresses of PDLSCs in vivo. If the application of appropriate TS can effectively expand PDLSCs, it will undoubtedly play a pivotal role in advancing both fundamental research and clinical practice. YAP is a key effector of the Hippo pathway, which is highly sensitive to mechanical stimuli. The role of YAP in cell proliferation and tissue regeneration has been widely confirmed [14, 15]. Recent studies have found that YAP participates in the fate regulation of PDLSCs under mechanical stimuli [3, 5]. As is well known, YAP typically undergoes nuclear translocation under the negative regulation of the Hippo pathway kinase cascade, thereby promoting the expression of downstream genes [16]. A study in 2019 suggested that YAP may be regulated by mechanisms independent of the Hippo pathway kinase cascade [36]. A 2023 study proposed that how YAP enters the nucleus in the mechanical microenvironment to control the fate and renewal of stem cells is still unknown [37]. Therefore, this study aimed to explore the appropriate conditions for TS to induce the proliferation of PDLSCs and to clarify the mechanical regulation mechanism of YAP nuclear translocation in promoting the proliferation of PDLSCs under TS.

Previous studies have shown that both internal and external physical forces can influence local mechanical

properties and cellular behavior via cytoskeletons [38, 39]. When cells are subjected to mechanical stimuli, the biomechanical and biochemical signals are ultimately transmitted through cytoskeletal complexes to the nucleus, thereby triggering relevant changes in cell function and gene expression [40]. Therefore, this study began with experiments of cytoskeletons to understand the mechanical response of PDLSCs under TS. Initially, we subjected PDLSCs to TS (12% elongation, 0.5 Hz) for 6 h or 24 h, using an in vitro tension system. We observed significant cytoskeleton remodeling, where F-actin became broader and denser, while microtubules redistributed widely around the nucleus. This may be due to the adaptive changes resulting from the TS pulling the cells. The nuclear area and nuclear pore size increased significantly, likely due to the enhanced and more divergent cytoskeletons exerting greater force on the nucleus. Further investigation revealed that 6 h of TS application promoted PDLSCs proliferation, whereas 24 h of continuous TS application resulted in the opposite result. This indicated that the positive response to mechanical stimulus may be time-sensitive, highlighting the need to maintain force application within an optimal timeframe to promote seed cell expansion.

YAP plays a pivotal role in the mechanical microenvironment of stem cells. Various biophysical stimuli from external forces, such as shear stress, extracellular matrix stiffness and adhesion area, can dictate stem cell fate by activating YAP [41–44]. A study found that oral squamous cell carcinoma cells promote their proliferation through the YAP/PIEZO1 axis [45]. Another study demonstrated that PPARα can activate and regulate the expression of YAP and its downstream target genes, regulating liver size and promoting regeneration [46]. Our research revealed that 6 h of TS application promoted YAP nuclear entry and upregulated the expression of proliferation-related genes. Conversely, YAP knockdown via siRNA rendered TS ineffective in promoting PDLSCs proliferation. These results confirmed that YAP directly participated in the regulation of PDLSCs proliferation under TS. The OTM model, known for its simple operation and stable results, can simultaneously capture the mechanical effects on both the TS side and the compression stress side, making it a popular choice as an animal model for verifying orthodontic force loading results in vitro [3, 47, 48]. Therefore, we constructed OTM models of SD rats to verify the reliability of in vitro experiments. The subsequent results indicated that the nuclear localization of YAP and the number of PCNA-positive cells in the tension side of PDL tissue increased over time after force application, peaking on the 7th day and normalizing by the 14th day. The in vivo experiments yielded the same results as the in vitro experiments, that is, appropriate TS promoted YAP nuclear translocation and subsequently cell proliferation. For in vivo conditions, sufficient PDLSCs proliferation was a prerequisite for the remodeling of PDL tissue.

The correlation between F-actin and YAP nuclear translocation has been explored in several studies [49, 50]. Gao et al. demonstrated that stress led to F-actin depolymerization, RhoA downregulation, and LPAR1 inactivation, facilitating YAP's cytoplasmic translocation through super-resolution imaging [49]. Li et al. confirmed that matrix stiffness could induce CD44-mediated YAP nuclear translocation in fibroblasts, requiring RhoA activity and F-actin cytoskeleton polymerization [50]. Our study further confirmed that the depolymerization of F-actin, rather than microtubules, greatly inhibited the nuclear translocation of YAP. The decrease in nuclear area and the increase in nuclear aspect ratio after adding CD indicated that nuclear shape was controlled by F-actin. It was confirmed that cell spreading and the stimulation of fibronectin can promote the formation of F-actin in the nucleus [51]. Our results revealed that TS not only promoted cytoplasmic F-actin expression but also upregulated the nuclear F-actin expression. This indicated that nuclear F-actin was highly sensitive to both physicochemical and mechanical stimuli. In short, these findings collectively affirmed that TS-induced YAP nuclear localization was strongly supported by F-actin dynamics.

The global actin organization played a significant role in direct cellular tension and focal adhesion regulation, yet the impact of actin organization on downstream signaling remains unclear [52]. The LINC complex, bridging the cytoplasmic and nuclear skeletons, anchors cytoskeletons to the nucleus, facilitating stable nuclear positioning [53, 54]. In non-muscle cells, the interaction between Nesprin1/2 and the actin cytoskeleton is emphasized [55, 56]. The LINC complex can act as both a direct mechanical sensor and a conduit for mechanical transduction to affect gene expression [57, 58]. However, the role of the LINC complex in YAP nuclear translocation has been less explored. In our in vitro part, 6 h of TS application upregulated the expression of the LINC complex; adding CD significantly reduced Nesprin1 expression, which indicated the expression of the LINC complex was dependent on F-actin dynamics. Adopting the methods of Denis and Zhang et al. [26, 31], we constructed an adenovirus (ADV-mCherry-DNKASH) that coupled mCherry to the overexpressed dominant negative KASH peptide of Nesprin1, to disrupt the LINC complex. Normally, Nesprin proteins bind to SUN proteins in the perinuclear space through the KASH domain. The

overexpressed dominant negative KASH peptide can bind to available binding sites on the SUN proteins, thereby replacing endogenous Nesprin proteins on the outer nuclear envelope [31, 59]. This adenovirus can replace all endogenous Nesprin proteins without causing compensation from other Nesprin subtypes [26]. The loss of Nesprin1 localization on the nuclear envelope in PDLSCs transfected with ADV-mCherry-DNKASH indicated that this method of disrupting the LINC complex was feasible. Our further results confirmed that the disrupted LINC complex inhibited TS-induced YAP nuclear translocation, thereby inhibiting YAP-regulated cell proliferation, indicating the indispensability of the LINC complex. The in vivo part also confirmed the disrupted LINC complex inhibited YAP nuclear localization and decreased cell proliferation in PDL tissue, thus hindering periodontal tissue remodeling and tooth movement. Our findings thoroughly demonstrate that the F-actin dynamics-dependent LINC complex was indispensable for TS-induced YAP nuclear translocation. Previous studies have described that YAP is highly sensitive to any mechanical deformation affecting the nucleus, and even a slight stretching can cause the transport from active to passive, given that the molecular weight of YAP is equal to the critical value of the nuclear pore complex when it is not deformed [25, 60, 61]. Their theory aligned with our results, further confirming the critical role of the LINC complex in transmitting TS to the nuclear envelope.

The functional response of mitochondria under TS needs to be confirmed. Our research discovered that the distribution of mitochondria was consistent with the distribution trend of microtubules, both under TS and with the addition of a microtubule inhibitor, supporting the fact that microtubules serve as tracks for mitochondrial transport within the cell [28, 62, 63]. Additionally, we observed that TS not only enhanced MMP but also activated mitochondrial dynamics. Previous studies have illustrated that mitochondrial localization shapes the cellular energy gradient to satisfy local energy demands [63, 64]. This led us to speculate whether these mitochondrial alterations were poised to supply energy for YAP nuclear translocation. ATP levels in PDLSCs significantly increased after TS application; however, adopting OA to inhibit intracellular ATP production significantly inhibited YAP nuclear translocation, thus confirming our conjecture. Studies have confirmed that cytoskeletons affect mitochondrial quality control, ATP production and calcium homeostasis [28]. Surprisingly, in our study, the polymerization intensity of F-actin decreased when intracellular ATP production was inhibited. This suggested a complex reciprocal interaction between mitochondria and cytoskeletons. However, inhibiting ATP synthesis did not seem to affect the cell projected area corresponding to F-actin, nor did it affect the expression of Nesprin1 under TS, indicating that there may exist more important factors driving F-actin polymerization under TS; warranting further investigation into the underlying mechanism.

There are still some limitations in this study. For instance, while we focused our discussion on the YAP nuclear translocation triggered by physical structures under TS, we neglected to explore the potential influence of biochemical responses on the distribution of YAP between the nucleus and cytoplasm. Additionally, the nuclear pore serves as the essential gateway for YAP to enter the nucleus. However, the potential changes in the composition and structure of the nuclear pore complex under TS have yet to be thoroughly investigated. All of these need to be further discussed in the follow-up research. Besides, although noteworthy outcomes were achieved in our animal experiments, large variations in tooth movement distances were observed among rats within the same group. These disparities could be attributed to disparities in the actual application of force as well as individual differences among the rats themselves. To acquire more reliable and stable findings, it is necessary to appropriately increase the sample size, while always maintaining ethical standards.

Taken together, we demonstrated that appropriate TS promoted PDLSCs proliferation via the mechanically driven F-actin/LINC complex/YAP axis (Fig. 7). TS augmented F-actin polymerization and stretching, which upregulated the expression of the LINC complex. This resulted in an increase in tension on the nuclear envelope, enlargement of the nuclear pore, and promotion of YAP entry into the nucleus, ultimately facilitating PDLSCs proliferation. Concurrently, mitochondria became active and migrated towards the nucleus along the reconstructed microtubules, supplying ATP for YAP nuclear translocation and, to a certain extent, driving F-actin polymerization. The indispensable role of the LINC complex was validated through both in vitro and in vivo experiments. Our findings confirmed that the application of appropriate TS was an effective method to expand PDLSCs. By precisely controlling strain magnitude and duration, PDLSCs proliferation can be promoted, and a healthy OTM environment can be maintained. We focused on elucidating the mechanical mechanism of TS-induced YAP nuclear translocation and could provide insights into the nuclear entry of other nuclear transcription factors under mechanical stress.

Conclusions

In this study, we have confirmed that the application of TS (12% elongation, 0.5 Hz) for 6 h in vitro can induce YAP nuclear translocation in PDLSCs, thereby promoting cell proliferation. The TS-induced YAP nuclear translocation was achieved through the polymerization of F-actin, upregulation of the LINC complex expression, tension transmission to the nuclear envelope and enlargement of nuclear pores, assisted by sufficient ATP. Our study can provide a theoretical basis for the expansion of seed cells in tissue engineering and the acceleration of tooth movement in orthodontic clinics, while also offering insights into the nuclear translocation of other nuclear transcription factors under mechanical stress.

Abbreviations

PDL	Periodontal Ligament
PDLSCs	Periodontal Ligament Stem Cells
TS	Tension Stress
OTM	Orthodontic Tooth Movement
YAP	Yes-Associated Protein
TEAD	Transcriptional Enhanced Associate Domain
LINC	Linker of Nucleoskeleton and Cytoskeleton
KASH	Klarsicht, ANC-1, and Syne Homology
SUN	Sad-1 and UNC-84
CD	Cytochalasin D
NO	Nocodazole
OA	Oligomycin A
MMP	Mitochondrial Membrane Potential
TEM	Transmission Electron Microscopy
PI	Proliferation Index
qRT-PCR	Quantitative Real-Time Polymerase Chain Reaction
siRNA	Small Interfering RNA
MOI	Multiplicity of Infection
ALP	Alkaline Phosphatase
micro-CT	Micro Computed Tomography
3D	Three-Dimensional
HE	Hematoxylin and Eosin
PCNA	Proliferating Cell Nuclear Antigen

Supplementary Information

The online version contains supplementary material available at https://doi.org/10.1186/s13287-024-03884-0.

Supplementary Material 1

Supplementary Material 2

Supplementary Material 3

Acknowledgements

Not applicable.

Author contributions

MX, ZL, and SJ designed the study. MX and ZY performed the experiments. MX, TH, and MY analyzed the data. LX, YG, and HX evaluated the data. MX wrote and edited the manuscript. DB, ZL, and SJ revised the work. All authors commented on the manuscript. All authors read and approved the final manuscript.

Funding

This work was supported by the National Natural Science Foundation of China (No. 82471016, No. 81470772); Chongqing Talent Program: Innovative leading talents (No. CQYC20210303384); Chongqing Medical Scientific Research Project (No. cstc2020jcyj-msxmX0307, No. CSTB2023NSCQ-MSX0233); Program for Youth Innovation in Future Medicine, Chongqing Medical University (No. W0033).

Data availability

All data supporting the conclusions of this article are included in the paper or supplementary information. Other relevant data are available from the corresponding author upon reasonable request.

Supplementary Information

Ethics approval and consent to participate

The extraction procedures of human PDLSCs were conducted in accordance with the Declaration of Helsinki, and informed consent was obtained from the donors and/or their guardians before the tooth collection. The animal experiments were conducted following the ARRIVE guidelines 2.0 (Animal Research: Reporting of In Vivo Experiments). The extraction procedures of human PDLSCs and all animal experiments in this study were approved by the Ethics Committee of Stomatological Hospital of Chongqing Medical University in the same project (Project title: Research on cytoskeleton mediated YAP nuclear translocation regulating the mechanical response mechanism of periodontal ligament stem cells; Approval No: 2023151; Date of approval: 2023-10-10).

Consent for publication

Not applicable.

Competing interests

The authors declare that they have no competing interests.

Author details

[1]College of Stomatology, Chongqing Medical University, Chongqing 401147, China
[2]Chongqing Key Laboratory of Oral Diseases, Chongqing 401147, China
[3]Chongqing Municipal Key Laboratory of Oral Biomedical Engineering of Higher Education, Chongqing 401147, China
[4]Oral Health Research and Promotion Unit, Al-Quds University, Jerusalem, Palestine

Received: 7 April 2024 / Accepted: 14 August 2024
Published online: 06 September 2024

References

1. Tomokiyo A, Wada N, Maeda H. Periodontal Ligament Stem cells: regenerative potency in Periodontium. Stem Cells Dev. 2019;28(15):974–85.
2. Wang L, Liang H, Sun B, Mi J, Tong X, Wang Y et al. Role of TRPC6 in periodontal tissue reconstruction mediated by appropriate stress. Stem Cell Res Ther. 2022;13(1).
3. Wang J, Yang H, Ma X, Liu J, Li L, Chen L, et al. LRP6/filamentous-actin signaling facilitates osteogenic commitment in mechanically induced periodontal ligament stem cells. Cell Mol Biol Lett. 2023;28(1):7.
4. Zhang D, Lin W, Jiang S, Deng P, Liu L, Wang Q et al. Lepr-expressing PDLSCs contribute to Periodontal Homeostasis and respond to Mechanical Force by Piezo1. Adv Sci. 2023;10(29).
5. Shi Q, Zheng L, Na J, Li X, Yang Z, Chen X et al. Fluid shear stress promotes periodontal ligament cells proliferation via p38-AMOT-YAP. Cell Mol Life Sci. 2022;79(11).
6. Brockhaus J, Craveiro RB, Azraq I, Niederau C, Schröder SK, Weiskirchen R, et al. In Vitro Compression Model for Orthodontic Tooth Movement Modulates Human Periodontal Ligament Fibroblast Proliferation, apoptosis and cell cycle. Biomolecules. 2021;11(7):932.
7. Li Y, Zhan Q, Bao M, Yi J, Li Y. Biomechanical and biological responses of periodontium in orthodontic tooth movement: up-date in a new decade. Int J Oral Sci. 2021;13(1).
8. Iskratsch T, Wolfenson H, Sheetz MP. Appreciating force and shape — the rise of mechanotransduction in cell biology. Nat Rev Mol Cell Biol. 2014;15(12):825–33.

9. Iwata T, Yamato M, Zhang Z, Mukobata S, Washio K, Ando T, et al. Validation of human periodontal ligament-derived cells as a reliable source for cytotherapeutic use. J Clin Periodontol. 2010;37(12):1088–99.
10. Mohebichamkhorami F, Fattahi R, Niknam Z, Aliashrafi M, Khakpour Naeimi S, Gilanchi S et al. Periodontal ligament stem cells as a promising therapeutic target for neural damage. Stem Cell Res Ther. 2022;13(1).
11. Shao X, Hu Z, Su H, Wang Y, Lin Y. Effects of tension on mitochondrial autophagy and osteogenic differentiation of periodontal ligament stem cells. Cell Prolif. 2023.
12. Sugimori T, Yamaguchi M, Shimizu M, Kikuta J, Hikida T, Hikida M, et al. Micro-osteoperforations accelerate orthodontic tooth movement by stimulating periodontal ligament cell cycles. Am J Orthod Dentofac Orthop. 2018;154(6):788–96.
13. Piccolo S, Dupont S, Cordenonsi M. The Biology of YAP/TAZ: Hippo Signaling and Beyond. Physiol Rev. 2014;94(4):1287–312.
14. Dupont S, Morsut L, Aragona M, Enzo E, Giulitti S, Cordenonsi M, et al. Role of YAP/TAZ in mechanotransduction. Nature. 2011;474(7350):179–83.
15. Azzolin L, Panciera T, Soligo S, Enzo E, Bicciato S, Dupont S, et al. YAP/TAZ incorporation in the beta-catenin destruction complex orchestrates the wnt response. Cell. 2014;158(1):157–70.
16. Romani P, Valcarcel-Jimenez L, Frezza C, Dupont S. Crosstalk between mechanotransduction and metabolism. Nat Rev Mol Cell Biol. 2020;22(1):22–38.
17. Aragona M, Panciera T, Manfrin A, Giulitti S, Michielin F, Elvassore N, et al. A mechanical checkpoint controls multicellular growth through YAP/TAZ regulation by actin-processing factors. Cell. 2013;154(5):1047–59.
18. Sansores-Garcia L, Bossuyt W, Wada K, Yonemura S, Tao C, Sasaki H, et al. Modulating F-actin organization induces organ growth by affecting the Hippo pathway. EMBO J. 2011;30(12):2325–35.
19. Crisp M, Liu Q, Roux K, Rattner JB, Shanahan C, Burke B, et al. Coupling of the nucleus and cytoplasm: role of the LINC complex. J Cell Biol. 2006;172(1):41–53.
20. Starr DA. KASH and SUN proteins. Curr Biol. 2011;21(11):R414–5.
21. Razafsky D, Hodzic D. Bringing KASH under the SUN: the many faces of nucleo-cytoskeletal connections. J Cell Biol. 2009;186(4):461–72.
22. Szczesny SE, Mauck RL. The Nuclear option: evidence implicating the cell nucleus in Mechanotransduction. J Biomech Eng. 2017;139(2):0210061–02100616.
23. Lombardi ML, Jaalouk DE, Shanahan CM, Burke B, Roux KJ, Lammerding J. The interaction between nesprins and sun proteins at the nuclear envelope is critical for force transmission between the nucleus and cytoskeleton. J Biol Chem. 2011;286(30):26743–53.
24. Tajik A, Zhang Y, Wei F, Sun J, Jia Q, Zhou W, et al. Transcription upregulation via force-induced direct stretching of chromatin. Nat Mater. 2016;15(12):1287–96.
25. Elosegui-Artola A, Andreu I, Beedle AEM, Lezamiz A, Uroz M, Kosmalska AJ, et al. Force triggers YAP Nuclear Entry by regulating transport across Nuclear pores. Cell. 2017;171(6):1397–e41014.
26. Denis KB, Cabe JI, Danielsson BE, Tieu KV, Mayer CR, Conway DE. The LINC complex is required for endothelial cell adhesion and adaptation to shear stress and cyclic stretch. Mol Biol Cell. 2021;32(18):1654–63.
27. Carley E, Stewart RM, Zieman A, Jalilian I, King DE, Zubek A et al. The LINC complex transmits integrin-dependent tension to the nuclear lamina and represses epidermal differentiation. Elife. 2021;10.
28. Shah M, Chacko LA, Joseph JP, Ananthanarayanan V. Mitochondrial dynamics, positioning and function mediated by cytoskeletal interactions. Cell Mol Life Sci. 2021;78(8):3969–86.
29. Huang H, Yang R, Zhou YH. Mechanobiology of Periodontal Ligament Stem Cells in Orthodontic Tooth Movement. Stem Cells Int. 2018;2018:6531216.
30. Zheng W, Wang S, Ma D, Tang L, Duan Y, Jin Y. Loss of proliferation and differentiation capacity of aged human periodontal ligament stem cells and rejuvenation by exposure to the young extrinsic environment. Tissue Eng Part A. 2009;15(9):2363–71.
31. Zhang Q, Narayanan V, Mui KL, O'Bryan CS, Anderson RH, Kc B, et al. Mechanical stabilization of the glandular acinus by Linker of Nucleoskeleton and Cytoskeleton Complex. Curr Biol. 2019;29(17):2826–e394.
32. Li H, Deng Y, Tan M, Feng G, Kuang Y, Li J et al. Low-intensity pulsed ultrasound upregulates osteogenesis under inflammatory conditions in periodontal ligament stem cells through unfolded protein response. Stem Cell Res Ther. 2020;11(1).
33. Huang H, Pan W, Wang Y, Kim HS, Shao D, Huang B, et al. Nanoparticulate cell-free DNA scavenger for treating inflammatory bone loss in periodontitis. Nat Commun. 2022;13(1):5925.
34. Martin-Martinez MD, Stoenoiu M, Verkaeren C, Devuyst O, Delporte C. Recombinant adenovirus administration in rat peritoneum: endothelial expression and safety concerns. Nephrol Dial Transpl. 2004;19(5):1293–7.
35. Seo B-M, Miura M, Gronthos S, Mark Bartold P, Batouli S, Brahim J, et al. Investigation of multipotent postnatal stem cells from human periodontal ligament. Lancet. 2004;364(9429):149–55.
36. Ma S, Meng Z, Chen R, Guan K-L. The Hippo Pathway: Biology and Pathophysiology. Annu Rev Biochem. 2019;88(1):577–604.
37. Driskill JH, Pan D. Control of stem cell renewal and fate by YAP and TAZ. Nat Rev Mol Cell Biol. 2023;24(12):895–911.
38. Fletcher DA, Mullins RD. Cell mechanics and the cytoskeleton. Nature. 2010;463(7280):485–92.
39. Svitkina T. The actin cytoskeleton and actin-based motility. Cold Spring Harb Perspect Biol. 2018;10(1).
40. Saucerman JJ, Tan PM, Buchholz KS, McCulloch AD, Omens JH. Mechanical regulation of gene expression in cardiac myocytes and fibroblasts. Nat Rev Cardiol. 2019;16(6):361–78.
41. Oliver-De La Cruz J, Nardone G, Vrbsky J, Pompeiano A, Perestrelo AR, Capradossi F, et al. Substrate mechanics controls adipogenesis through YAP phosphorylation by dictating cell spreading. Biomaterials. 2019;205:64–80.
42. Kim N-G, Koh E, Chen X, Gumbiner BM. E-cadherin mediates contact inhibition of proliferation through Hippo signaling-pathway components. Proc Natl Acad Sci U S A. 2011;108(29):11930–5.
43. Xue X, Hong X, Li Z, Deng CX, Fu J. Acoustic tweezing cytometry enhances osteogenesis of human mesenchymal stem cells through cytoskeletal contractility and YAP activation. Biomaterials. 2017;134:22–30.
44. Hu JK, Du W, Shelton SJ, Oldham MC, DiPersio CM, Klein OD. An FAK-YAP-mTOR signaling Axis regulates stem cell-based tissue Renewal in mice. Cell Stem Cell. 2017;21(1):91–106. e6.
45. Hasegawa K, Fujii S, Matsumoto S, Tajiri Y, Kikuchi A, Kiyoshima T. YAP signaling induces PIEZO1 to promote oral squamous cell carcinoma cell proliferation. J Pathol. 2021;253(1):80–93.
46. Fan S, Gao Y, Qu A, Jiang Y, Li H, Xie G, et al. YAP-TEAD mediates PPAR alpha-induced hepatomegaly and liver regeneration in mice. Hepatology. 2022;75(1):74–88.
47. Wang C, Yang Q, Han Y, Liu H, Wang Y, Huang Y, et al. A reduced level of the long non-coding RNA SNHG8 activates the NF-kappaB pathway by releasing functional HIF-1alpha in a hypoxic inflammatory microenvironment. Stem Cell Res Ther. 2022;13(1):229.
48. Zhang Z, Cui S, Fu Y, Wang J, Liu J, Wei F. Mechanical force induces mitophagy-mediated anaerobic oxidation in periodontal ligament stem cells. Cell Mol Biol Lett. 2023;28(1).
49. Gao J, He L, Zhou L, Jing Y, Wang F, Shi Y, et al. Mechanical force regulation of YAP by F-actin and GPCR revealed by super-resolution imaging. Nanoscale. 2020;12(4):2703–14.
50. Li S, Li C, Zhang Y, He X, Chen X, Zeng X, et al. Targeting mechanics-Induced Fibroblast activation through CD44-RhoA-YAP pathway ameliorates crystalline silica-Induced Silicosis. Theranostics. 2019;9(17):4993–5008.
51. Plessner M, Melak M, Chinchilla P, Baarlink C, Grosse R. Nuclear F-actin formation and reorganization upon cell spreading. J Biol Chem. 2015;290(18):11209–16.
52. Wen SM, Wen WC, Chao PG. Zyxin and actin structure confer anisotropic YAP mechanotransduction. Acta Biomater. 2022;152:313–20.
53. Zhu R, Antoku S, Gundersen GG. Centrifugal displacement of nuclei reveals multiple LINC complex mechanisms for Homeostatic Nuclear Positioning. Curr Biol. 2017;27(20):3097–110. e5.
54. Heffler J, Shah PP, Robison P, Phyo S, Veliz K, Uchida K, et al. A Balance between Intermediate filaments and microtubules maintains Nuclear Architecture in the cardiomyocyte. Circ Res. 2020;126(3):e10–26.
55. Luxton GW, Gomes ER, Folker ES, Vintinner E, Gundersen GG. Linear arrays of nuclear envelope proteins harness retrograde actin flow for nuclear movement. Science. 2010;329(5994):956–9.
56. Luxton GWG, Gomes ER, Folker ES, Worman H, Gundersen GG. TAN Lines Nucleus. 2014;2(3):173–81.
57. Alam SG, Zhang Q, Prasad N, Li Y, Chamala S, Kuchibhotla R, et al. The mammalian LINC complex regulates genome transcriptional responses to substrate rigidity. Sci Rep. 2016;6:38063.
58. Wang N, Tytell JD, Ingber DE. Mechanotransduction at a distance: mechanically coupling the extracellular matrix with the nucleus. Nat Rev Mol Cell Biol. 2009;10(1):75–82.

59. Mayer CR, Arsenovic PT, Bathula K, Denis KB, Conway DE. Characterization of 3D printed stretching devices for Imaging Force transmission in live-cells. Cell Mol Bioeng. 2019;12(4):289–300.
60. Saporito S, Natale CF, Menna C, Netti PA, Ventre M. A role for nuclear stretching and NPCs changes in the cytoplasmic-nuclear trafficking of YAP: an experimental and numerical modelling approach. Mater Today Bio. 2022;15:100335.
61. Matsuda A, Mofrad MRK. On the nuclear pore complex and its emerging role in cellular mechanotransduction. APL Bioeng. 2022;6(1).
62. Bartolak-Suki E, Imsirovic J, Nishibori Y, Krishnan R, Suki B. Regulation of mitochondrial structure and Dynamics by the Cytoskeleton and mechanical factors. Int J Mol Sci. 2017;18(8).
63. Yang C, Svitkina TM. Ultrastructure and dynamics of the actin-myosin II cytoskeleton during mitochondrial fission. Nat Cell Biol. 2019;21(5):603–13.
64. Schuler M-H, Lewandowska A, Caprio GD, Skillern W, Upadhyayula S, Kirchhausen T, et al. Miro1-mediated mitochondrial positioning shapes intracellular energy gradients required for cell migration. Mol Biol Cell. 2017;28(16):2159–69.

Publisher's note